CrossMark

ORIGINAL PAPER

Leaning pagodas in China: laboratory test and analysis of subsidence under frequent earthquakes

Yong Jing Tang[1,2] · Yong Zhao[1]

Abstract The inclination of ancient pagodas leads to a non-uniform stress distribution on the soil below. This non-uniform stress threatens the structural stability of the ancient pagodas, and the degree of damage depends on the soil properties. This paper researches the residual strain under the ancient pagodas in China to simulate the non-uniform stress state under frequent earthquake conditions using a dynamic triaxial test apparatus. The non-uniform stress state was expressed by the consolidation stress ratio. The frequent earthquakes were indicated by the dynamic stress ratio and cyclic interval vibration loading. To describe the foundations of the ancient pagodas in China, two types of soil, the mucky clay (Q_4) and the paleo-clay (Q_3^{al}), were tested. The relationship between the two different soils and the consolidation and dynamic stress ratios were determined by measuring the deformation and accumulated deformation. Additionally, mathematical models to estimate the residual strains of the soils were established and verified. The results indicate that the soil strain increment of mucky clay, which increases with the consolidation stress ratio and dynamic stress ratio, is an important parameter for evaluating the leaning pagodas' stability in soft soil regions when subjected to frequent earthquake. The soil strain increment of paleo-clay, however, is inversely proportional to the consolidation stress ratio and no apparent relationship is found with the dynamic stress ratio. More research needs to be done on the subsidence of paleo-clay.

✉ Yong Jing Tang
  ytang@tongji.edu.cn

[1] Department of Geotechnical Engineering, Tongji University, 1239 Siping Road, Shanghai 200092, China

[2] Key Laboratory of Geotechnical and Underground Engineering, Ministry of Education, Tongji University, 1239 Siping Road, Shanghai 200092, China

Introduction

Ancient Chinese pagodas, referred to as the high-rise buildings in old times, are tubular structures. Unlike modern high-rise buildings, most of these pagodas were built on shallow foundations. The primitive construction methodology used in ancient times created an initial inclination of the pagodas. In addition, ancient Chinese pagodas have endured long-term wind loads and periodic nondestructive earthquakes (i.e., frequent earthquakes, of which exceeding probability in 50 years is 63%) (Chinese National Standard 2010) over their long service periods. Therefore, the existing pagodas nowadays exhibit varying degrees of inclination. The tilt of these pagodas causes non-uniform stress distributions in the ground under their shallow foundations. Furthermore, additional differential settlements caused by the non-uniform stress distributions influence the stability and safety of these pagodas.

The non-uniform stress distribution and differential settlements can be divided into two parts: those resulting from the dead and daily live loads, which have accumulated over long-term service and those resulting from dynamic loads, such as frequent earthquakes, which have significantly contributed to the additional inclination of the pagodas. For instance, an additional 1.5° of tilt in the Leaning Tower of Pisa, with constant weight, occurred between 1278 and 1360 (Burland et al. 1998); this was tentatively attributed to the five earthquakes that occurred in 1279, 1322 and between 1325 and 1345.

🖄 Springer

Chen et al. (2008), François et al. (2010), Yan et al. (2012) and Yılmaz et al. (2004) address the soil dynamics with accumulated deformation caused by subway vibrations and the permanent deformation of soil below buildings and infrastructures resulting from rare earthquakes. However, differential soil settlements caused by frequent earthquakes, considering non-uniform stress levels, are rarely reported. No previous studies have used laboratory tests to research the non-uniform settlements of cohesive clays for ancient pagodas under frequent earthquake conditions from the soil mechanics point-of-view.

The differential deformations of foundation clays caused by frequent earthquakes and non-uniform stress levels are main factors in estimating the safety and stability of ancient pagodas. The additional inclination of the pagodas, which will increase the stress on the masonry, occurs because of the differential deformations of the soil foundation. The Leaning Tower of Pisa research demonstrated that the normal compressive stress of the masonry increased at approximately 7 kPa per second of arc and the hoop stress increased at approximately 1.8 kPa per second of arc (Zhou et al. 2001). Besides, the additional inclination of the pagodas will significantly affect the stability of the soil foundation (Burland et al. 1998). However, previous researchers did not pay much attention to differential deformations of soil foundations. In 1996, the belfry of Foligno Town Hall in Italy collapsed in an earthquake (Beconcini et al. 2001). The bell tower, similar to ancient Chinese pagodas, featured tubular structures. Investigations into the causes of collapse were conducted after the accident. The relevant references are limited to features such as the towers' masonry properties, the perpendicular stress on the bodies and the heat sensitivities (Baronio et al. 1997; Binda et al. 1997, 1998), ignoring the foundation functions despite foundations being key elements of the tower. More recently, Abruzzese et al. (2009) researched the famous Huzhu Pagoda in Shanghai, which leans one degree more than Pisa's tower, without considering the soil foundation either.

Consequently, the study of the accumulated deformations under the tilt situation of pagodas is critically important to evaluate pagodas' stability. Accumulated deformation can be used to estimate the additional inclination caused by non-uniform stress under frequent earthquakes, which will increase the stress on the masonry in ancient pagodas and threaten their foundation stability. The non-uniform stress distribution in the foundation soil caused by the initial inclination of pagodas results in different consolidation stress ratios of foundation soil units. This paper investigates the residual strains of foundation soil units with different consolidation stress ratios under equivalent frequent earthquake load using a dynamic triaxial test apparatus. According to the difference of residual strains of foundation soil units, the accumulated deformation of foundation soil under the ancient pagodas, which is available for predicting the additional inclination of ancient pagodas under frequent earthquakes, can be calculated.

Experimental method

Testing material

Soil samples from the foundation-bearing stratum were taken from Shanghai where the Longhua Pagoda (Fig. 1) is located and from An-qing where the Zhenfeng Pagoda (Fig. 2) is located. Shanghai, where estuarine delta marine strata develop, is a platform depression on the northeast verge of Yangtze para-platform and close to the Circum-Pacific Seismic Belt Area. An-qing, where fluvial facies/lacustrine facies strata develop, is a basin on the east verge of the frontal arc of the Huaiyang epsilon structural system and close to the Tanlu Fault. The two cities (Fig. 3) lie on the edge of an earthquake region and often experience small-amplitude earthquakes. The Longhua Pagoda (E121°26′50.61″, N31°10′32.29″, Elevation +4 m) is located in Xuhui District in Shanghai. It was first built in 247 for Buddhist use and rebuilt in 977. It has seven stories and eight sides and was built of brick masonry and wood. The brick pagoda wall functions as the main supporting member of the structure and the wooden corner beams, rafters and bucket arches constitute the eaves. The Longhua Pagoda is 15,187 kN in weight, 40.60 m high and has a 2 m deep brick foundation. The leaning angle is now 1.36° northward and 0.55° eastward. The maximum settlement is 991.5 mm at the top center of the pagoda (Chen 2012). The Zhenfeng Pagoda (E117°02′57.13″, N30°30′12.69″, Elevation +4 m) is located in the city of An-qing in An-hui Province. It was first built in 1570 for Buddhist use and as a navigation aid. It has seven stories and eight sides and was built of brick masonry. The Zhenfeng Pagoda is 52,015 kN in weight, 60.86 m high and has a 1 m deep eight-edge stone foundation of 18.72 m per side (Tang et al. 2010). The leaning angle is now 0°7′1″ in the southwest direction and the maximum settlement is 36.00 mm (Tang and Wang 2016). Both of the two pagodas are in the lists of the Sixth Batch of China National Key Protected Cultural Relic Organizations. The Longhua Pagoda is not open to the tourists while Zhenfeng Pagoda is a tourist spot nowadays.

The foundation-bearing stratum properties differ between Shanghai and An-qing. The former features typical mucky clay and the latter features paleo-clay. Employing a dynamic triaxial test apparatus, the accumulated deformation of the soil samples was measured under different consolidation stress ratios and dynamic stress
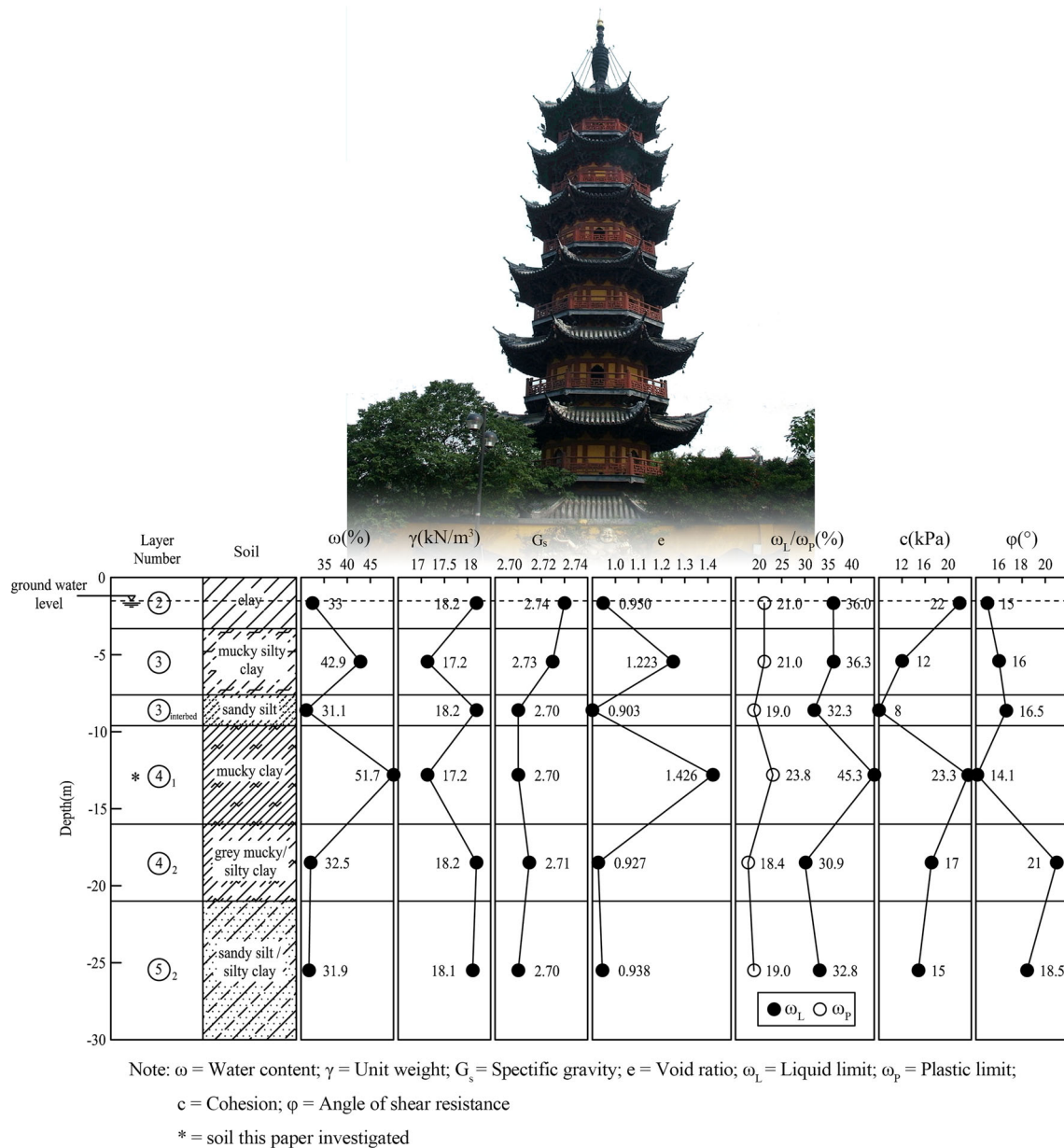
Fig. 1 An illustrative geotechnical profile and properties of foundation soil under the Longhua Pagoda

ratios to model non-uniform stress levels under frequent earthquakes.

Triaxial dynamic apparatus

The dynamic triaxial tests were conducted in the Key Laboratory of the Education Ministry in the Department of Geotechnical Engineering, Tongji University. A geotechnical digital systems (GDS) dynamic triaxial test apparatus produced by GDS Instruments in Britain, as shown in Fig. 4a, was used. The apparatus is composed of a pressure system, a measuring system and a control system. The pressure system is supported by a back pressure controller (provides pore water pressure and back pressure and control volumetric strain), a cell pressure controller (provides cell pressure) and an axial pressure controller (provides axial pressure and control axial deformation). The measuring system can read and save radial/axial strain and pore water pressure through internal sensors (e.g., Hall Effect Sensor).The control system includes geotechnical digital system laboratory software, an automatic digital control and collection system. Other parameters of this apparatus are as follows: a maximum confining pressure of 1 MPa, a frequency range of 0–5 Hz, a maximum axial force of 10 kN, a deformation of ± 25 mm and a strain of 10^{-4} to 10^{-2}.The specimen diameter and height are 39.1 and 80.0 mm, respectively, as shown in Fig. 4b.
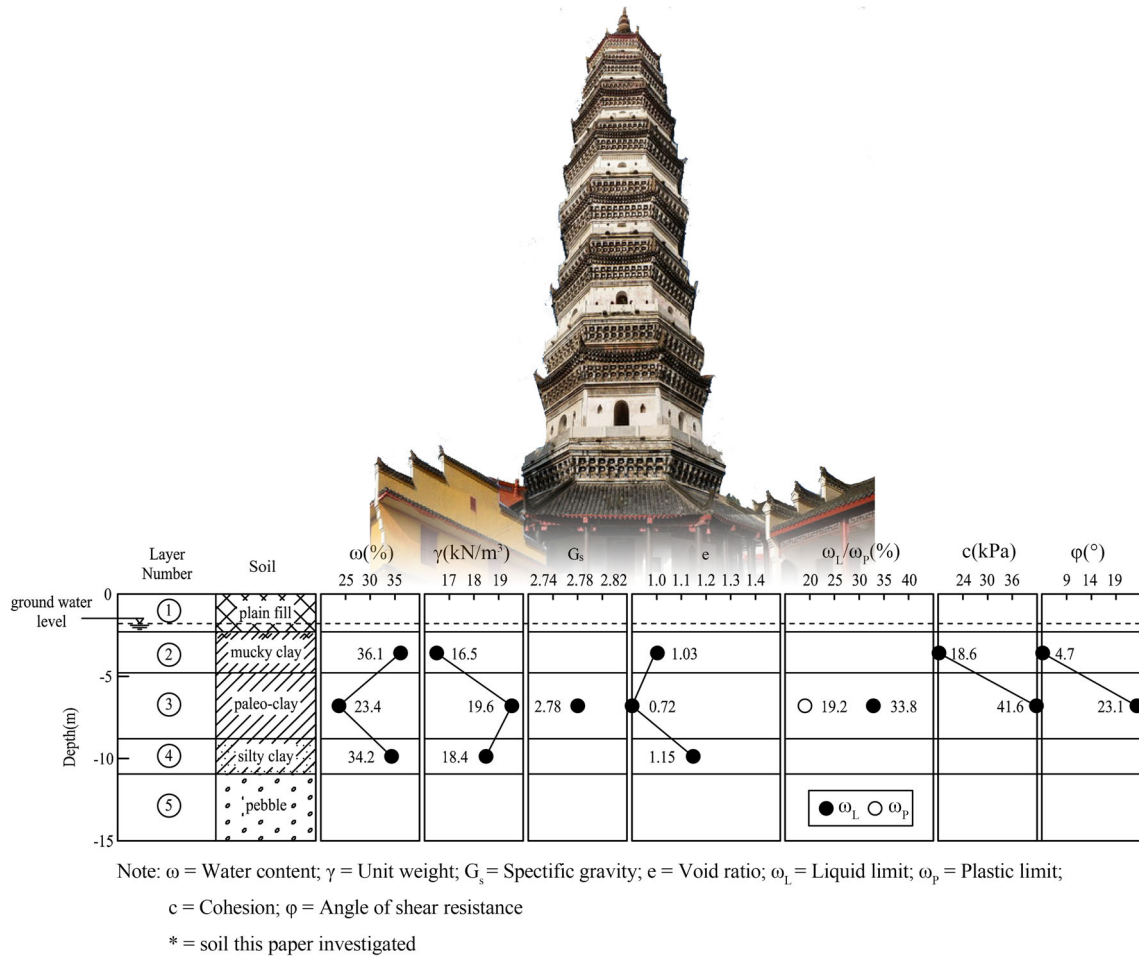
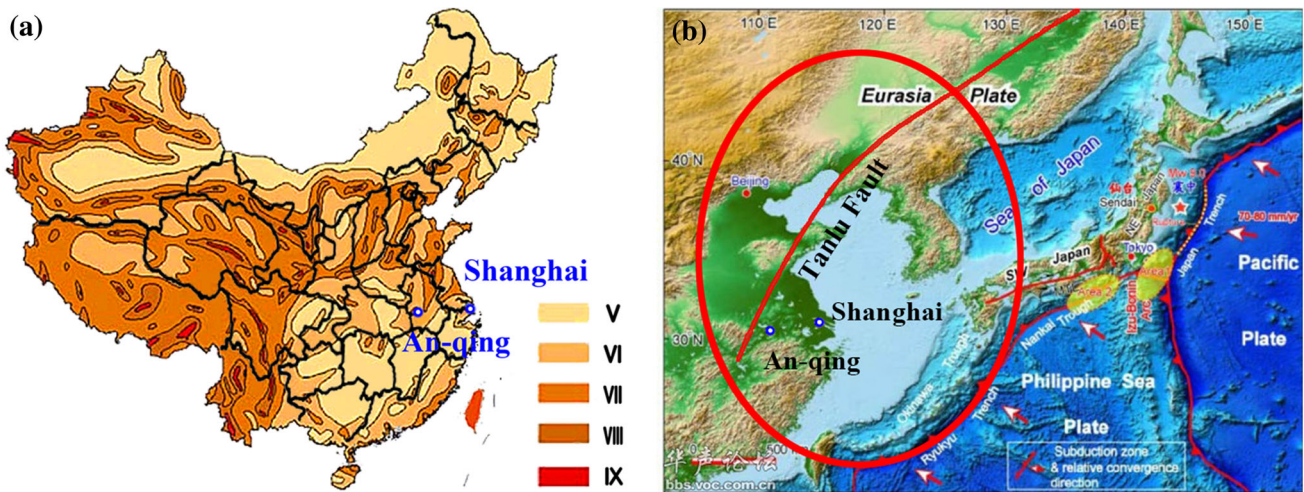Fig. 2 An illustrative geotechnical profile and properties of foundation soil under the Zhenfeng Pagoda

Fig. 3 Seismological sketch of the areas of Shanghai and An-qing **a** The earthquake intensity zoning map of China; **b** the location of Shanghai, An-qing and the nearby earthquake regions

Experimental preparation

Soil samples from Shanghai, the mucky clay, are Quaternary Holocene soil (Q_4). These samples were taken from

$④_1$ layer soil in Shanghai, 12–15 m below the ground, and are a very soft, gray, soft-plastic clay with silty sand. Soil samples from An-qing, paleo-clay, are Quaternary Pleistocene soil (Q_3^{al}). They are from approximately 5–8 m

**Fig. 4** Dynamic traxial test apparatus and sample **a** Dynamic traxial test apparatus; **b** sample
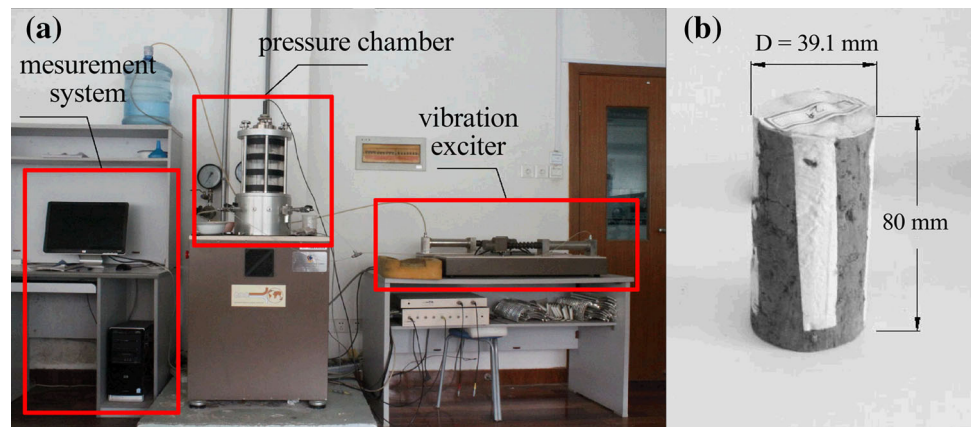
below the ground and are reddish-brown, hard plastic with small rocks. Selected physical and mechanical properties of the soils are listed in Figs. 1 and 2. All samples were wrapped with wax in the field and transported directly to the Key Laboratory of the Education Ministry in the Department of Geotechnical Engineering, Tongji University. With the standard method (Chinese National Standard 1999), the undisturbed samples were formed into 39.1 mm diameter pieces and placed into a half-circular steel mold. Next, 80.0 mm long specimens were cut.

Before a sample was put into the pressure cell, all the conduits were filled with water to exhaust air. Filter papers and porous plates were put on the top and bottom surfaces of the sample and four filter paper strips were attached on the cylindrical surface. The sample was wrappedwith rubber membrane and fastened to the sample cap and the pedestal of the pressure cell. The cover of the pressure cell was closed and inject water was injected. Then backpressure saturation was initiated according to predetermined parameters and test procedures. The test procedures included backpressure saturation, consolidation, loading and reconsolidation. The consolidation stage consisted of the isotropic consolidation step and the anisotropic consolidation step, each of which required 12 h. To avoid intensity failure during the anisotropic consolidation step, each stress was maintained below 20 kPa. Once the pore water pressure stabilized, the consolidation stage was considered finished. The test loading stage involved loading equivalent vibrations on the soil specimens. The reconsolidation stage included an undrained reconsolidation step and a drained reconsolidation step, each of which required 2 or 3 h. The experimental processes can be seen as Fig. 5.

Experimental scheme to simulate the original inclination of the ancient pagodas

We often assume that the consolidation stress ratios of soil at identical depths and in one location are equivalent. In
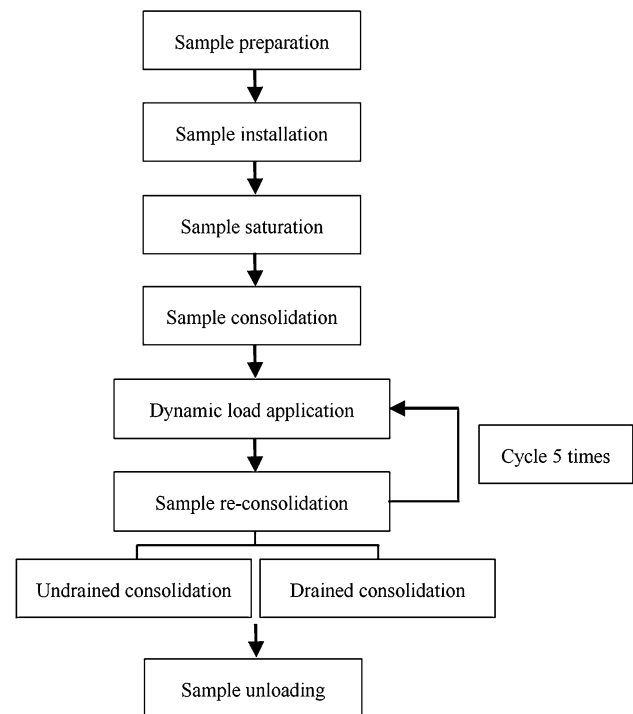
Fig. 5 Experimental processes

fact, because of the non-uniform stress caused by the original inclination of pagodas, the consolidation stress ratio of the sub-soil at identical depths varies. The soil experiencing the larger stress should have a larger consolidation stress ratio value and a smaller stress would correspond to a smaller consolidation stress ratio value. In this study, different sub-soil consolidation stress ratio values were considered to simulate the present inclination of ancient pagodas.

Based on the real stress states and consolidated-drained conditions, the isotropic and anisotropic consolidation stresses are determined. After considering the non-uniform stress function of the soil under the ancient pagodas and the difference in the stress state of the soil between the two

regions in Shanghai and An-qing, the consolidation stress ratios K_c, defined as axial pressure/confining pressure (σ_1/σ_3), are taken as 1.2, 1.4 and 1.6 for the mucky clays in Shanghai and 1.2, 1.25, 1.4, 1.6, 2.2 and 2.5 for the paleo-clay in An-qing.

The experimental scheme for the Shanghai mucky clay and the An-qing paleo-clay is detailed in Table 1.

Experimental scheme to simulate the frequent earthquakes

The residual deformation from the loading and reconsolidation stages consists of three parts: part 1 results from the equivalent earthquake-induced vibration in the loading stage; part 2 results from the undrained residual strain after vibration in the reconsolidation stage; and part 3 results from the drained residual strain in the reconsolidation stage. One complete residual deformation round is comprised of the three parts described above. In the tests, the loading stage is to measure part 1 and the undrained consolidation step in the reconsolidation stage is for part 2. Both of these processes are to simulate instantaneous deformation of soil caused by undrained residual strain under the earthquakes. The drained consolidation step in the reconsolidation stage is for part 3. It means to simulate reconsolidation deformation due to dissipation of excess pore water pressure after the earthquakes. During the tests, the total residual deformation is the result of loading and reconsolidation. Herein, we assumed that loading and reconsolidation rounds are five. The five rounds are used to simulate the additional residual strain on the ancient pagodas subject to five frequent earthquakes during their long service period.

Table 1 Test scheme for Shanghai and An-qing soil

Sample	Consolidation period		Vibration period		Reconsolidation period			Note
	σ_3 (kPa)	σ_1 (kPa)	T (h)	σ_d (kPa)	f (Hz)	T_{CU} (h)	T_{CD} (h)	
$S_{1.2}^{0.025}$	100	120	24	5	1	3	3	Note 1
$S_{1.2}^{0.03}$	100	120		6	1			
$S_{1.2}^{0.03'}$	100	120		6	1			
$S_{1.2}^{0.05}$	100	120		10	1			
$S_{1.2}^{0.09}$	100	120		20	1			
$S_{1.4}^{0}$	100	140	24	0	0	0	0	Note 3
$S_{1.4}^{0.03}$	100	140		6	1	2 h	2 h	Note 1
$S_{1.4}^{0.05}$	100	140		10	1	3 h	3 h	Note 1
$S_{1.4}^{0.09}$	100	140		22	1	2 h	2 h	Note 1
$S_{1.6}^{0.03}$	100	160	24	6	1	3 h	3 h	Note 1
$S_{1.6}^{0.05}$	100	160		10	1	3 h	3 h	Note 1
$S_{1.6}^{0.09}$	100	160		24	1	3 h	3 h	Note 1
$S_{1.6}^{0.09'}$	100	160		24	1	2 h	2 h	Note 1
$C_{1.2}^{0.14}$	120	144	24	36	1	3	3	Note 1
$C_{1.25}^{0.07}$	120	150		19.2	1			Note 1
$C_{1.25}^{0.13'}$	100	125		30	1			Note 1
$C_{1.25}^{0.13}$	120	150		36	1			Note 1
$C_{1.25}^{0.118}$	120	150		48	1	2	2	Note 1
$C_{1.25}^{0.18}$	120	150		48	1	3	3	Note 1
$C_{1.4}^{0.13}$	120	168		36	1	3	3	Note 1
$C_{1.4}^{0.14'}$	120	168		36	1	0	0	Note 2
$C_{1.6}^{0.14}$	100	160		36	1	3	3	Note 1
								Note 1
$C_{1.6}^{0.14'}$	100	160		30	1			Note 1
$C_{2.2}^{0.05}$	150	264		19.2	1			Note 1
								Note 1

Note 1: five-round load amplitude of vibration and reconsolidation. Note 2: 100 continuous cycles. Note 3: samples without vibration

S represents the mucky clay, C represents the paleo-clay, upper script for dynamic stress ratio R, lower script for consolidation stress ratio, T, T_{CU} and T_{CD} for consolidation time before cyclic vibration, undrained consolidation time and drained consolidation time after cyclic vibration, respectively, and σ_d and f for the stress amplitude and frequency of the harmonic vibration of a sinusoidal wave

In the tests, a regular sinusoidal wave is adopted to simulate the vibration of frequent earthquakes. The amplitude and frequency are determined by the local earthquake intensity and equivalent principle (Seed 1979). Ignoring the structure-soil interaction between the ancient pagodas and the sub-soil foundations, the simplified shear stress amplitude of the equivalent harmonic wave (τ_e) is expressed in Eq. (1).

$$\tau_e = 0.65\gamma_d \frac{\gamma h}{g}\alpha_{max}, \tag{1}$$

where γ_d is the stress reduction coefficient and varies with depth as described in Table 2, γ is the unit weight of the soil, h is the depth of the soil stratum below the ground, α_{max} is the measured maximum acceleration and g is the acceleration of gravity.

The dynamic stress ratio, R, is defined by Eq. (2) based on reference (Seed and Chan 1966).

$$R = \sigma_d/(\sigma_1 + \sigma_3), \tag{2}$$

where σ_d is the calculated dynamic amplitude value ($\sigma_d = 2\tau_e$) and σ_1 and σ_3 are the axial pressure and the confining pressure, respectively.

According to the Chinese National Standard (2010), the seismic precautionary intensity (earthquake intensity with exceeding probability of 10% in 50 years) of Shanghai and An-qing is 7.0 and the design basic acceleration of ground motion is 0.1 g. As for frequent earthquakes (earthquake intensity with exceeding probability of 63% in 50 years), the simplified shear stress amplitude of the equivalent harmonic wave (τ_e) would be multiplied by a reduction coefficient. According to the calculations of formula (1) and (2), the dynamic stress ratio varies from 0.02 to 0.11. For one group of specimens, R is set as 0 for reference, corresponding to no vibration. In the loading stage, the vibration time is set as 20 s according to the Chinese National Standard (2015) and the vibration frequency as 1 Hz on the basis of spectrum analysis of local earthquakes and previous research, which indicate that the fields in Shanghai and An-qing have a selective effect on the frequency spectrum of acceleration of ground motion. With this effect, the low frequency component is amplified and long-period content is prominent. The reconsolidation stage follows the dynamic loading stage, requiring 4–6 h (2–3 h for the undrainage step and 2–3 h for the drainage step). Five vibration-reconsolidation rounds are performed on each specimen in the tests.

Test results and analysis

Mucky clay in Shanghai

The correlation coefficient of the accumulated residual strain and dynamic stress ratio is less than that of the accumulated residual strain and consolidation stress ratio. The relationship between the accumulated residual strain and consolidation stress ratio under different dynamic stress ratios is illustrated in Fig. 6. The maximum accumulated strain is 1.24% for dynamic stress ratios $R \leq 0.09$ and consolidation stress ratios $K_c \leq 1.6$. Nevertheless, the residual strain has not reached the turning point, i.e., the critical value, which suggests the occurrence of damage and reconstitution of the soil structure. The residual strain increases with the dynamic stress ratio, whereas the connection between the accumulated strain and consolidation stress ratio shows a more apparent trend. The maximum variation in the residual strain is $1.17 - 0.46 = 0.71\%$ for dynamic stress ratio $R = 0.05$, and the minimum is $1.24 - 0.75 = 0.46\%$ for $R = 0.09$ (Table 3). According to the experiments and data above, assuming that the deformation of mucky clay is the main deformation of the foundation soil under the ancient pagoda, an expected additional inclination of the ancient pagoda under frequent earthquakes can be calculated. As for the Longhua Pagoda (Chen 2012), the foundation diameter is 6.66 m. As shown from the test data in Table 4, when $R = 0.05$, the maximum differential residual strain is 0.71% at the ends. Assuming that the thickness of the compressible soil layer is 15 m, and the body of the pagoda is rigid, the inclination of the ancient pagoda is calculated by the layer-by-layer summation method (Stolyarov 2011), expressed in Eq. (3). The Longhua Pagoda will incur an additional inclination of 1.60%. Thus, the deformation of the structure will increase, ultimately shortening the life of the pagoda.

$$i = \sum_{j=1}^{n}\left(\varepsilon_{K_C^{j1}}^{R} - \varepsilon_{K_C^{j2}}^{R}\right) \times h_j/L, \tag{3}$$

where i is the inclination increment; $\varepsilon_{K_C^{j1}}^{R}$ and $\varepsilon_{K_C^{j2}}^{R}$ ($j = 1, ..., n$) are the residual strains of the soil of layer j at two points, K_C^{j1} and K_C^{j2}, respectively, as shown in Fig. 7, h_j is the compression thickness in layer j of the soil and L is the distance in layer j between the points K_C^{j1} and K_C^{j2}. Herein, L is taken as the equivalent diameter of the pagoda's foundation.

In Fig. 8, it can be observed that the residual strain increases with K_c and R. The axial residual strain is also

Table 2 Stress reduction coefficient

Depth (m)	0	1.5	3.0	4.5	6.0	7.5	9.0	10.5	12.0
γ_d	1.000	0.985	0.975	0.965	0.955	0.935	0.915	0.895	0.856
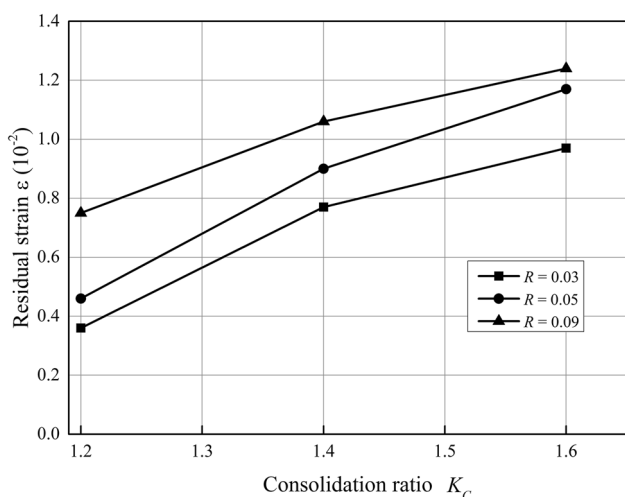
Fig. 6 Residual strain vs. consolidation ratio curves for mucky clay

Fig. 7 Sketch of the soil parameters

shown under different cases. The strain accumulates in the reconsolidation period, which includes the undrained and drained reconsolidation phases. During the drained reconsolidation phase, the accumulated residual strain significantly increases.

Figure 9 shows the residual strain of mucky clay caused by the vibration of 100 continuous cycles and five rounds of 20 cycles. The residual strain increment during the intervals in the tests under interval vibrations have been cut down. The residual strain caused by continuous vibrations is less than that caused by interval vibrations.

Paleo-clay in An-qing

Figure 10 shows that the residual strain of clay decreases as the consolidation stress ratio K_c increases. The dynamic stress ratio is ignored here because of its insignificant influence. The value of the residual strain is less than that for the mucky clay, as shown in Fig. 6.
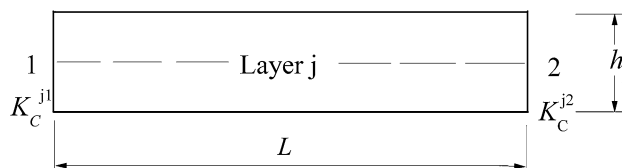
Figure 11 shows that the residual strain varies by load case and consolidation stress ratio when the dynamic stress ratio is 0.11. Paleo-clay exhibits a stable residual strain development compared with mucky clay (Fig. 8). The residual strain is much smaller than that for mucky clay and no apparent relationship is found with the consolidation stress ratio. As shown from the test data in Table 4, when $R = 0.09$, the maximum differential accumulated residual strain is 0.043%. As for the Zhenfeng Pagoda (Tang et al. 2010), the circumscribed circle diameter of the foundation is 21.00 m and the thickness of the compression layer of the soil is 42 m, twice the circumscribed circle diameter of the foundation. By Eq. (3), the maximum differential accumulated residual strain only produces an additional inclination of approximately 0.086%.

Figure 12 shows the residual strain of paleo-clay caused by the vibration of 100 continuous cycles and five rounds of 20 cycles. The residual strain increment during the intervals also has been cut down. The residual strain from the continuous vibration is ultimately larger than that caused by the interval vibration. The residual strain exhibits the opposite trend for mucky clay, as shown in Fig. 9.

Regression models and verification

Mathematical model for mucky clay

The test data for Shanghai mucky clay listed in Table 3 illustrates that the correlation coefficient between the

**Table 3** Accumulated residual strain ($\times 10^{-2}$) for Shanghai mucky clay

Data type	$K_c = 1.2$ $R = 0.03$	$K_c = 1.4$ $R = 0.03$	$K_c = 1.6$ $R = 0.03$	$K_c = 1.2$ $R = 0.05$	$K_c = 1.4$ $R = 0.05$	$K_c = 1.6$ $R = 0.05$	$K_c = 1.2$ $R = 0.09$	$K_c = 1.4$ $R = 0.09$	$K_c = 1.6$ $R = 0.09$
Test	0.36	0.77	0.97	0.46	0.90	1.17	0.75	1.06	1.24
Fitting	0.35	0.78	1.01	0.48	0.88	1.10	0.74	1.07	1.26

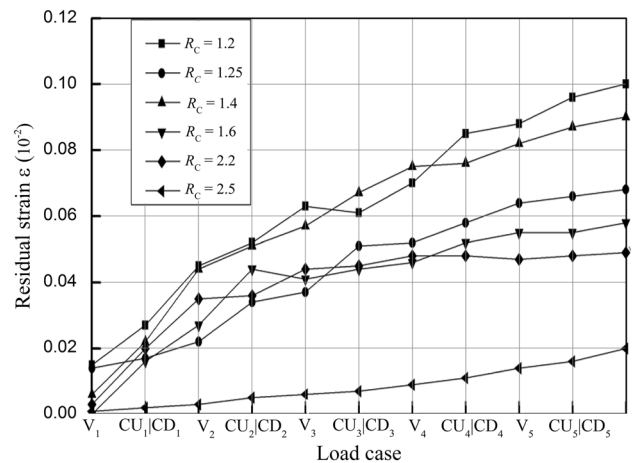**Table 4** Accumulated strain ($\times 10^{-3}$) for paleo-clay

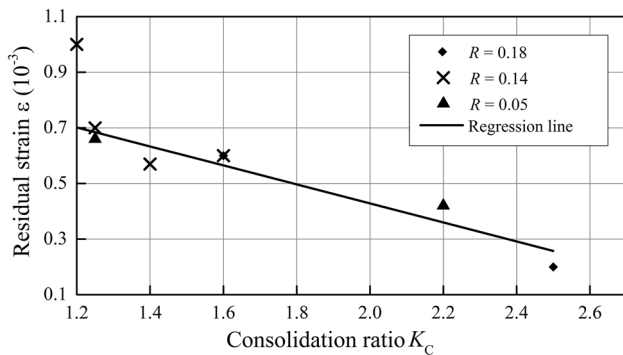| Data type	$R = 0.09$ $K_c = 1.2$	$R = 0.09$ $K_c = 1.25$	$R = 0.05$ $K_c = 1.25$	$R = 0.09$ $K_c = 1.4$	$R = 0.09$ $K_c = 1.6$	$R = 0.11$ $K_c = 1.6$	$R = 0.05$ $K_c = 2.2$	$R = 0.11$ $K_c = 2.5$
Test	1.00	0.70	0.66	0.57	0.60	0.60	0.42	0.20
Fitting	0.70	0.68	0.68	0.63	0.56	0.56	0.36	0.25

Fig. 8 Residual strain vs. various conditions and case curves for mucky clay
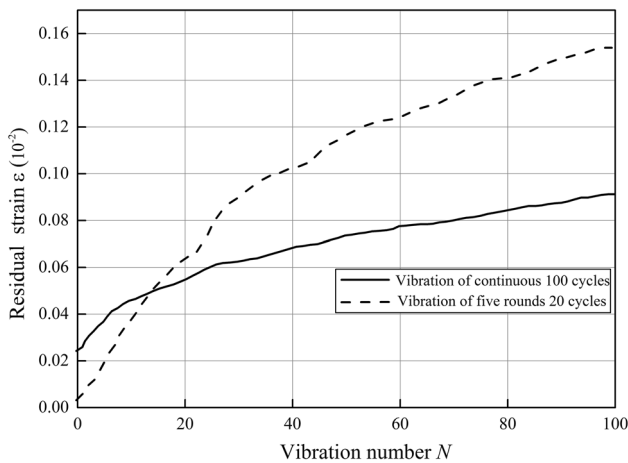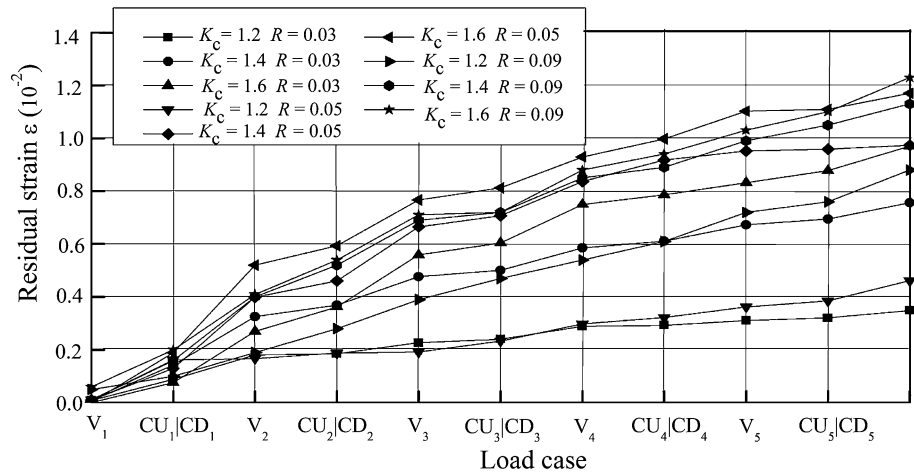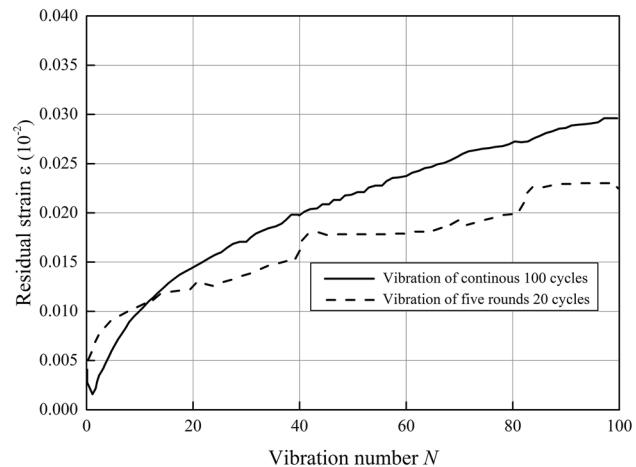

Fig. 9 Residual strain vs. vibration number curves for mucky clay

Fig. 10 Residual strain vs. consolidation ratio K_c for paleo-clay

Fig. 11 Residual strain vs. various conditions and case curves for paleo-clay

Fig. 12 Residual strain vs. vibration number curves for paleo-clay

accumulated residual strain and the consolidation stress ratio is larger than the dynamic stress ratio. Therefore, the mathematical model is constructed using a two-layer method. The first layer involves the consolidation stress ratio and the second layer involves the dynamic stress ratio. Using the data from columns (2)–(4), (5)–(7) and (8)–(10) in Table 3, the coefficients of the quadratic equation expressed in Eq. (4) are

listed in Table 5. Next, the relationships between the coefficients in Eq. (4) are regressed (expressed as micro strain, $\varepsilon \times 10^{-2}$) and expressed in Eq. (4a).

$$\varepsilon = a_0 + a_1 K_c + a_2 K_c^2, \tag{4}$$

$$\begin{aligned} a_0 &= -7.9146 + 44.9640R, \\ a_1 &= 10.3630 - 51.2500R, \\ a_2 &= -3.0357 + 16.0710R, \end{aligned} \tag{4a}$$

where ε is the accumulated strain, K_c is the consolidation stress ratio and R is the dynamic stress ratio.

Mathematical model for paleo-clay

It should be noted that the influence of the dynamic stress ratio on the residual strain for the paleo-clay could be ignored, as shown in Fig. 10. Thus, the mathematical model can be expressed in Eq. (5) (expressed as micro strain, $\varepsilon \times 10^{-3}$).

$$\varepsilon = -0.3416 K_c + 1.1115. \tag{5}$$

Goodness of fit and significance tests

The statistical index for assessing goodness of fit is expressed in Eq. (6).

$$R^2 = SS_e / SS_r, \tag{6}$$

where R^2 is the statistical index for assessing the fit, $SS_e = \sum_{i=1}^{n} (y_i - \widehat{y_i})^2$ and $SS_r = \sum_{i=1}^{n} (\widehat{y_i} - \bar{y})^2$. Here, y_i is the test value of the accumulated strain, $\widehat{y_i}$ is the fit value of the accumulated strain and $\bar{y}$ is the average test value of the accumulated strain.

For linear equations, the F test can be used to test the significance of models (Sheng et al. 2008). The statistical index F is expressed in Eq. (7).

$$\begin{cases} F = \dfrac{\dfrac{SS_r}{\sigma^2}/2}{\dfrac{SS_e}{\sigma^2}/(n-3)} = \dfrac{SS_r}{SS_e/(2n-6)} & \text{for mucky clay} \\[4mm] F = \dfrac{\dfrac{SS_r}{\sigma^2}}{\dfrac{SS_e}{\sigma^2}/(n-2)} = \dfrac{SS_r}{SS_e/(n-2)} & \text{for } Q_3^{al} \text{ clay,} \end{cases} \tag{7}$$

For a given level of significance, Eq. (8) describes the probability of the event.

$$\begin{cases} P(F > f_{2,n-3}) = \alpha & \text{for mucky clay} \\ P(F > f_{1,n-2}) = \alpha & \text{for } Q_3^{al} \text{ clay} \end{cases}, \tag{8}$$

where P is probability, F is the statistical index, n is the number of degrees of freedom and α is the level of significance, which is assumed to be 0.05.

The critical value can be found using the F distribution in Table 6.

For mucky clay, $n = 3$ and $\alpha = 0.05$ and the critical value is 18.51. From Eq. (7), $F(a_0) = 344.82$, $F(a_1) = 555.55$, so $F > 18.51$, thus satisfying the requirement for Eq. (4a).

For paleo-clay, $n = 8$ and $\alpha = 0.05$, and the critical value is 5.59. From Eq. (7), $F = 162.24 > 5.59$, satisfying the requirement for Eq. (5).

The goodness of fit and significance test results are listed in Table 6, whereas the test and fitting data are compared for mucky clay and paleo-clay in Tables 3 and 4, respectively.

Tables 3, 4, 5 and 6 indicate that the analysis results obtained from the tests and by using the models are consistent.

Assume that $K_c^2 = K_c'$, where K_c' is a parameter instead of square term K_c^2, then Eq. (4) can be considered as a linear regression model. Next, the equivalent equation can be verified using the F significance test.

Qualitative verification

Pellegrinelli et al. (2014) conducted a similar study of non-uniform subsidence of soil foundations of ancient pagodas caused by earthquakes. The practical data will be used to qualitatively verify Eq. (4).

Pellegrinelli et al. studied the leaning bell tower of San Benedetto Church in Ferrara in Italy. It had overhangs of 2.85 and 0.50 m along the west and north, respectively, in 2011. The poor mechanical properties of the sub-soil below the leaning tower's foundation (Pellegrinelli et al. 2014) are similar to those of the mucky clay in Shanghai. Pellegrinelli et al. placed four benchmarks on the corners of the leaning tower (C1, C2, C3 and C4) and two reference benchmarks on the adjacent San Benedetto Church (C5 and C6), as shown in Fig. 13.

Because the tower leans westward, the stress of the soil under the edge along C1 and C2 is greater than the stress of

Table 5 Coefficients for Eq. (4)

R	a_0	a_0 (fitting)	a_1	a_1 (fitting)	a_2	a_2 (fitting)
0.03	−6.5100	−6.5657	8.8750	8.8255	−2.4650	−2.5538
0.05	−5.7500	−5.6664	7.7250	7.8005	−2.2250	−2.2322
0.09	−3.8400	−3.8678	5.7750	5.7505	−1.6250	−1.5893

Table 6 Goodness of fit and significance test results

Model description		SS_e	SS_r	Goodness of fit	F statistical index	F critical value
Mathematical model for Eq. (4a), coefficients of consolidation ratio and dynamic stress ratio for mucky soils	a_0	0.01086	3.78487	0.0029	344.82	18.51
	a_1	0.00875	4.91167	0.0018	555.55	18.51
	a_2	0.01286	0.37561	0.0342	29.20	18.51
Mathematical model for accumulated strain, consolidation ratio, and dynamic stress ratio for paleo-clay		0.0033	0.0893	0.0370	162.24	5.59

$SS_e = \sum_{i=1}^{n} (y_i - \hat{y_i})^2$ and $SS_r = \sum_{i=1}^{n} (\hat{y_i} - \bar{y})^2$ are described in Eq. (7).

the soil under the edge along C3 and C4, so are the consolidation stress ratios. After the earthquake, a sudden subsidence of benchmarks C1 and C2 was indicated of -2.6 mm, while for C3 and C4, with a smaller consolidation stress ratio value, no variations were observed. The result is qualitatively consistent with Eq. (4), and there is a positive correlation between the accumulated strain and consolidation stress ratio.

Discussion of soil subsidence

According to the previousresearch, the causes of soil subsidence can be classified into four parts.

1. *Constitutive property* The constitutive properties of soil differ from kind to kind, thus causing the reactions

Fig. 13 The benchmark distribution of the leaning bell tower of San Benedetto Church in Italy (Pellegrinelli et al. 2014)

to dynamic loadings to vary. For example, the thixotropic properties of soft clay makes it hard to restore the original structure once it is broken by dynamic loadings (Yu and Shi 1989).

2. *Softening effect* By dynamic triaxial tests, Thiers and Seed (1969) found that the static elastic modulus of soil under dynamic loadings is smaller than it is without loadings. Due to the increase of pore water pressure and the decrease of effective stress, the static elastic modulus drops, and the soil becomes "softer".

3. *Inertia effect* The shear stress in the soil increase under the earthquakes. The inertia force will cause part of the soil to slide and eventually increase the accumulated plastic deformation (Yu et al. 1996).

4. *Reconsolidation* After the earthquake, with the dissipation of excess pore water pressure, the reconsolidation deformation is generated.

The subsidence of one kind of soil can be caused by the combination of reasons above due to its physical and mechanical indices.

Mucky clay and paleo-clay, differing in constitutive, water content, cohesion and so on, exhibit radically different reactions. The pore water pressure of mucky clay increases mainly after the equivalent earthquake-induced vibration and dissipates at the drainage consolidation stage. The pore water pressure of paleo-clay remains basically stable in the vibration-reconsolidation process (Tang and Zhao 2012).

Mucky clay causes large subsidence, and the accumulated residual strain in mucky clay increases with the consolidation stress ratio. These can be attributed to the high saturation, high water content and sensitive constitutive properties. With the increase of the consolidation stress ratio, water drainage increases. Monismith et al. (1975) described similar findings. With a higher consolidation stress ratio, the structure of mucky clay begins to change and plastic deformation occurs easily under dynamic load.

The relationship between accumulated residual strain and consolidation stress ratio of paleo-clay had a reserved trend against mucky clay. Paleo-clay features low saturation and stable constitutive properties. More researches on
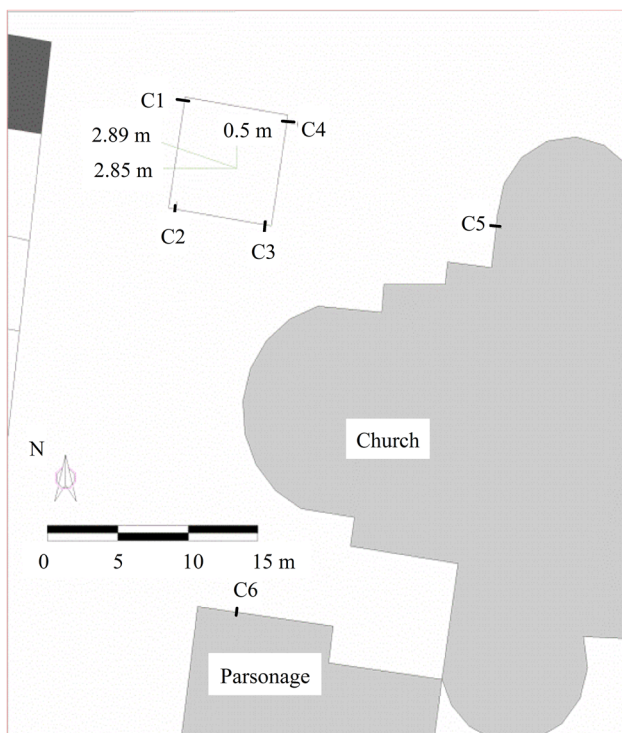
over-consolidation ratio, material composition and other properties are required to explain the subsidence of paleo-clay.

Residual strain caused by continuous vibration in mucky clay is smaller than that caused by interval vibration. By contrast, residual strain caused by continuous vibration in paleo-clay is larger than that by interval vibration. The tests under interval vibration and continuous vibration mean to distinguish the influence on soil of vibration caused by multi-frequency earthquakes and continuous vibration. More researches need to be done on the interpretation of experimental results.

Besides, when calculating the additional inclination of the ancient pagoda, it is under the assumption that the deformation of soil this paper researched (mucky clay and paleo-clay) is the main deformation of the foundation soil, and the structure-soil interaction is ignored. To achieve more accurate prediction results, the deformation property of soil from other soil layers under the ancient pagoda needs to be researched. Finite element codes, such as SOFIA, could be used to evaluate the structure-soil interaction to present accurate boundary conditions (Cavallaro et al. 2003), which helps to acquire more reliable results of dynamic triaxial tests. Furthermore, to ensure the stabilization of ancient pagodas, investigations on foundation rectification, superstructure reinforcement and deformation monitoring can be conducted.

Conclusions

Triaxial dynamic tests have demonstrated that the accumulated residual strains of mucky clay in Shanghai increase with the dynamic stress ratios and consolidation stress ratios. The relationship between the accumulated strains of paleo-clay and the dynamic stress ratios is not significant and may be ignored.

Tests have shown that the residual strain of mucky clay in Shanghai resulting from continuous vibrations is less than resulting from interval vibrations. By contrast, the residual strain of the paleo-clay in the city of An-qing, An-hui Province resulting from continuous vibrations is greater than that resulting from interval vibrations.

Based on the analyses for mucky clay, the differential strain increments, which lead to the additional inclination increment of the pagoda body, are important indices for estimating the structural stability of ancient pagodas.

Consequently, since soil properties are the factors contributing to soil collapse caused by earthquakes under the ancient pagodas, protecting the soil underneath the ancient pagodas, particularly through timely consolidation and drainage, is important.

References

Abruzzese D, Miccoli L, Yuan JL (2009) Mechanical behavior of leaning masonry Huzhu Pagoda. J Cult Herit 10(4):480–486

Baronio G, Binda L, Lombardini N (1997) The role of brick pebbles and dust in conglomerates based on hydrated lime and crushed bricks. Constr Build Mater 11(1):33–40

Beconcini ML, Bennati S, Salvatore W (2001) Structural characterisation of a medieval bell tower: first historical, experimental and numerical investigations. In: Proceedings of the 3rd international seminar, structural analysis of historical constructions, historical constructions 2001, possibilities of numerical and experimental techniques, Guimarães, Portugal, pp 431–444

Binda L, Mondena C, Baronio G, Abbaneon S (1997) Repair and investigation techniques for stone masonry walls. Constr Build Mater 11(3):133–142

Binda L, Lenzi G, Saisi A (1998) NDE of masonry structures: use of radar tests for the characterization of stone masonries. NDT&E Int 31(6):411–419

Burland JB, Jamiolkowski M, Viggiani C (1998) Stabilising the leaning tower of Pisa. Bull Eng Geol Environ 57(1):91–99

Cavallaro A, Massimino MR, Maugeri M (2003) Noto cathedral: soil and foundation investigation. Constr Build Mater 17(8):533–541

Chen HM (2012) Inspection and finite element analysis of the Longhua Tower, Shanghai, a protected structure. Hous Sci 33(5):35–38 **(in Chinese)**

Chen GX, Zhu DH, Shi JJ, Liu XZ (2008) Test on earthquake-induced permanent deformation of Nanjing recently deposited muddy soil. In: Proceedings of 2nd international conference for disaster mitigation and rehabilitation, Nanjing, Springer, Hong Kong, pp 301–308

Chinese National Standard: GB 50011 (2010) Seismic design of buildings. China Building Industry Press, Beijing

Chinese National Standard: GB/T 50123 (1999) Standard for soil test method. China Planning Press, Beijing

Chinese National Standard: GB/T 50269 (2015) Measurement methods of dynamic properties of subsoil. China Planning Press, Beijing

François S, Karg C, Haegeman W, Degrande G (2010) A numerical model for foundation settlements due to deformation accumulation in granular soils under repeated small amplitude dynamic loading. Int J Numer Anal Meth Geomech 34:273–296

Monismith CL, Ogawa N, Freeme CR (1975) Permanent deformation characteristics of subgrade soils due to repeated loading. Transp Res Rec 537:1–17

Pellegrinelli A, Furini A, Russo P (2014) Earthquakes and ancient leaning towers: geodetic monitoring of the bell tower of San Benedetto Church in Ferrara (Italy). J Cult Herit 15(6):687–691

Seed HB (1979) Soil liquefaction and cyclic mobility evaluation for level ground during earthquakes. J Geotech Eng Div 105(2):201–255

Seed HB, Chan CK (1966) Clay strength under earthquake loading condition. J Soil Mech Found Div 92(SM2):53–78

Sheng J, Xie SQ, Pan CY (2008) Probability and statistics. Higher Education Press, Beijing **(in Chinese)**

Stolyarov VG (2011) Calculation of bed settlement by the method of layer-by-layer summation in accordance with building code 51-101-2004 and the method of integration. Soil Mech Found Eng 48(2):67–72

Tang YJ, Wang SH (2016) A new approach based on plane and circular fitting to survey the axial shape and assess the inclination of ancient Chinese pagodas. KSCE J Civil Eng 20(5):2014–2021

Tang YJ, Zhao WS (2012) Triaxial test research on dynamic settlement of ancient architecture foundation soil under frequent earthquakes. J Tongji Univ (Nat Sci) 40(10):1486–1490 **(in Chinese)**

Tang YJ, Shao ZD, Kujawski E (2010) Zhenfeng tower maintenance and its durability. In: Banthia N, Mufti A (Eds.) Conservation of heritage structures, proceedings of the third international workshop on civil structural health monitoring, The University of British Columbia, Vancouver, Canada, pp 421–428

Thiers GR, Seed HB (1969) Strength and stress-strain characteristics of clays subjected to seismic loading conditions. Vib Eff Earthq Soils Found 450:3–56

Yan CL, Tang YQ, Wang YD, Ren XW (2012) Accumulated deformation characteristics of silty soil under the subway loading in Shanghai. Nat Hazards 62(2):375–384

Yılmaz MT, Pekcan O, Bakır BS (2004) Undrained cyclic shear and deformation behavior of silt–clay mixtures of Adapazarı, Turkey. Soil Dyn Earthq Eng 24(7):497–507

Yu SS, Shi ZJ (1989) Soil seismic subsidence research. Chin J Geotech Eng 11(4):35–44 **(in Chinese)**

Yu HZ, He GN, Yang B (1996) Seismic subsidence research of soft soil. J Dalian Univ Technol 36(1):76–82 **(in Chinese)**

Zhou Z, Ogot M, Schwartz L (2001) A finite element analysis of the effects of an increasing angle on the tower of Pisa. Finite Elem Anal Des 37(11):901–911